First Result of a Paraphoton Search with Intense X–ray Beams at SPring–8

T. Inada[1], *T. Namba*[2], *S. Asai*[1], *T. Kobayashi*[2],
Y. Tanaka[3], *K. Tamasaku*[3], *K. Sawada*[3], *T. Ishikawa*[3]

[1]Department of Physics, Graduate School of Science, the University of Tokyo, Japan
[2]International Center for Elementary Particle Physics, the University of Tokyo, Japan
[3]Spring-8/RIKEN Harima Institute, Kouto, Sayo-cho, Sayo-gun, Hyogo, Japan

DOI: http://dx.doi.org/10.3204/DESY-PROC-2013-04/inada_toshiaki

We present our first result of a search for paraphotons with *a light shining through a wall* (LSW) method at SPring–8. An intense synchrotron radiation from a long undulator beamline is used to search for paraphotons whose mass is in X–ray region. No excess of events above background is observed, and a stringent constraint is obtained on the photon–paraphoton mixing angle, $\chi < 8.06 \times 10^{-5}$ (95% C.L.) for $0.04\,\mathrm{eV} < m_{\gamma'} < 26\,\mathrm{keV}$. Results as well as plans for the next phase are presented.

1 Introduction

Many extensions of the Standard Model contain extra $U(1)$ symmetries [1]. If SM matter is uncharged in the additional $U(1)$ symmetry, the $U(1)$ gauge bosons are referred to as paraphotons, or hidden sector photons. Paraphotons have tiny mixing with ordinary photons through very massive particles which have both electric and hidden charge [2]. This effective mixing term induces flavor oscillations between paraphotons and ordinary photons [3]. With this oscillation mechanism, a high sensitive search can be done with a method called *a light shinning through a wall* (LSW)[4], in which incident photons oscillate into paraphotons that are able to pass through a wall and oscillate back into photons.

Recently, a detailed theoretical study of the photon and axion-like particle conversion probability has been performed[5]. Since both axion– and paraphoton–conversion are described as the same quantum oscillations, the conversion probability for axions can be interpreted as that of paraphotons by replacing parameters from $\frac{\beta\omega}{m^2}$ to χ in Eq. (29) in [5]. After propagation in vacuum for length L, the probability of converting a paraphoton into a photon (or vice versa) is given by,

$$p_{\gamma\leftrightarrow\gamma'}(L) = \left(\frac{\omega + \sqrt{\omega^2 - m_{\gamma'}^2}}{\sqrt{\omega^2 - m_{\gamma'}^2}}\chi\right)^2 \sin^2\left(\frac{L}{2}\left(\omega - \sqrt{\omega^2 - m_{\gamma'}^2}\right)\right), \tag{1}$$

where χ is the mixing angle, $m_{\gamma'}$ is the mass of the paraphoton, and ω is the energy of photon. For low mass region ($m_{\gamma'} \ll \omega$), it becomes a well-known expression of a neutrino-like oscillation; $p_{\gamma\leftrightarrow\gamma'}(L) = 4\chi^2 \sin^2(m_{\gamma'}^2 L/4\omega)$.

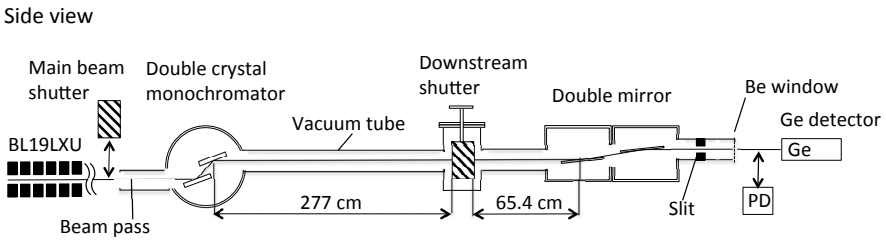

Figure 1: Schematic view of our experimental setup.

Up to now, paraphoton searches with the LSW method have mainly used optical sources [6] or microwave sources [7]. Since the accessible maximum mass of paraphoton is limited to the energy of incident photons, a higher-energy source extends the mass upper limit of LSW experiments. Furthermore, terrestrial sources in an X–ray region provide a new possibility to paraphoton searches since these experiments can be a test of parameter space probed by astrophysics only.

Here, we report a new search for paraphotons with the LSW method. We use an intense X–ray beam created by a long undulator at SPring–8 synchrotron radiation facility to search paraphotons whose mass is in the (10^{-1}–10^{4}) eV region.

2 Experimental Setup

We used BL19LXU [8] beamline at SPring–8 (Fig. 1) as X–ray source. A 30-m long undulator is placed on the electron storage ring as shown in Fig. 1. A bunch length of electrons in the storage ring is 40 ps, and a bunch interval is 23.6 ns. Structure of a X–ray beam represents the bunch structure of electrons, but we regard it as a continuous beam because time resolution of X–ray detector is larger than this structure. An energy of the X–ray beam is tunable between 7.2 and 18 keV by changing a gap width of the undulator. Higher energy of its 3rd harmonics (21.6 $\sim$ 51 keV) is also available. X–ray beam is monochromated with a Si(111) double crystal monochromator to the level of $\Delta\omega/\omega \sim 10^{-4}$. A reflection angle is determined from Bragg condition, and is typically $\sim$ 100 mrad for energies we use. A beam size is about 1 mm, and a vertical profile ($\rho(x)$) is measured with a slit with 10 μm pitch. Shape of $\rho(x)$ is similar to Gaussian whose FWHM is 383 μm.

The X–ray beam from the monochromator is guided through vacuum tubes, whose length is about 3.5 m. Tubes are evacuated better than 4×10^{-5} Pa, and a double mirror is placed at the downstream edge of the tube. These mirrors are adjusted for the total reflection, and their reflection angle is tuned at 3.0 mrad (or 2.0 mrad) during our search (only at 26 keV search). They serve as a beam-pass filter, since only X–ray beams satisfying a severe condition of total reflection are bounced up and the other off-axis background photons are blocked. The X–ray beam changes its path with these mirrors and only the reflected beam is selected with a slit, and guided to the X–ray detector.

There are two beam shutters placed in the beamline. Main Beam Shutter (MBS) is placed just before the monochromator, and DownStream Shutter (DSS) is placed between the monochromator and the mirrors. Photon changes into paraphoton in a vacuum tube between the monochromator and DSS, and then changes back inversely in the region between DSS and

beam energy ω (keV)	livetime (10^4 s)	detector resolution σ (keV)	event rate in $(\omega \pm 2\sigma)$ N (10^{-3} s^{-1})	BG subtracted rate in $(\omega \pm 2\sigma)$ ΔN (10^{-4} s^{-1})	signal upper limit ΔN_{95} (10^{-4} s^{-1})	beam flux I (10^{13} s^{-1})	detector efficiency ϵ (%)	LSW prob. upper limit P_{95} (10^{-16})
7.27	2.5	0.16	7.0 ± 0.5	-0.9 ± 5.7	11.0	7.6	23	0.63
8.00	2.0	0.16	6.5 ± 0.6	-3.8 ± 6.1	10.3	8.9	33	0.35
9.00	3.2	0.17	5.3 ± 0.4	-7.6 ± 4.5	5.5	8.3	46	0.14
15.00	1.9	0.18	4.2 ± 0.5	-3.4 ± 5.0	8.2	4.6	51	0.35
16.00	2.1	0.18	4.2 ± 0.4	-3.1 ± 4.8	7.9	3.7	56	0.38
17.00	2.5	0.18	4.2 ± 0.4	-2.1 ± 4.5	7.8	2.3	61	0.56
21.83	2.5	0.19	4.2 ± 0.4	$+4.2 \pm 4.3$	12.2	0.72	76	2.2
23.00	2.0	0.20	3.9 ± 0.4	$+1.2 \pm 4.7$	10.5	0.43	78	3.1
26.00	2.6	0.21	4.8 ± 0.4	$+7.6 \pm 4.6$	15.6	1.3	83	1.4

Table 1: Summary of 9 measurements of the paraphoton search. Errors are one standard deviation statistical errors.

the mirrors. Each length at the beam center is (277 ± 2) cm and (65.4 ± 0.5) cm, respectively.

We used a germanium detector (Canberra BE2825) to detect X–ray signal. A diameter and thickness of its crystal is 60 mm and 25 mm, respectively. Signal of Ge detector is shaped with an amplifier (ORTEC 572) and recorded by a peak hold ADC (HOSHIN C-011). Energy resolution of the detector is measured with ^{55}Fe, ^{68}Ge, ^{57}Co, and ^{241}Am sources, and typical energy resolution at 10 keV is 0.17 keV (σ: standard deviation). Absolute efficiencies of the X–ray detector (ϵ) are also measured by the same sources. Measured efficiencies are consistent with GEANT4 Monte Carlo results, which includes all attenuations in the air, carbon composite window (thickness= 600 μm) of the detector, and surface dead layer (thickness = (7.7 ± 0.9) μm) of the germanium crystal.

The detector is shielded by lead blocks whose thickness is about 50 mm except for a collimator on the beam axis whose hole diameter is 30 mm, much larger than the X–ray beam size. The position of the collimator and the germanium crystal against the beam is adjusted by using a photosensitive paper which is sensitive to the X–ray.

Absolute flux of the X–ray beam and its stability are monitored by a silicon PIN photodiode (Hamamatsu S3590-09, thickness = 300 μm). This photodiode is inserted in front of the collimator of the lead shield, and DSS is opened for the flux measurement. During this measurement, the collimator hole is closed to avoid the radiation damage to the germanium detector. The energy deposited on the PIN photodiode is calculated using its output current and the W-value of silicon (W = 3.66 eV). Fraction of the X–ray energy deposition in the PIN photodiode is computed with GEANT4 simulation for each energy. To correct the saturation effect of the PIN photodiode, thin aluminum foils are inserted before the photodiode to attenuate X–ray flux. Attenuation coefficient of aluminum is also checked by GEANT4 simulation. The flux can be measured with an accuracy of less than 5%.

3 Measurement and Analysis

A paraphoton search is performed during our beamtime from 14th to 20th June, 2012. 9 measurements are performed with different X–ray energies from 7.27 keV to 26.00 keV. Results are summarized in Tab. 1. Beam intensities (I) are monitored every 3–4 hours by the PIN photodiode as described in the previous section. Energy calibration of the detector is also performed every 3–4 hours with a ^{57}Co source.

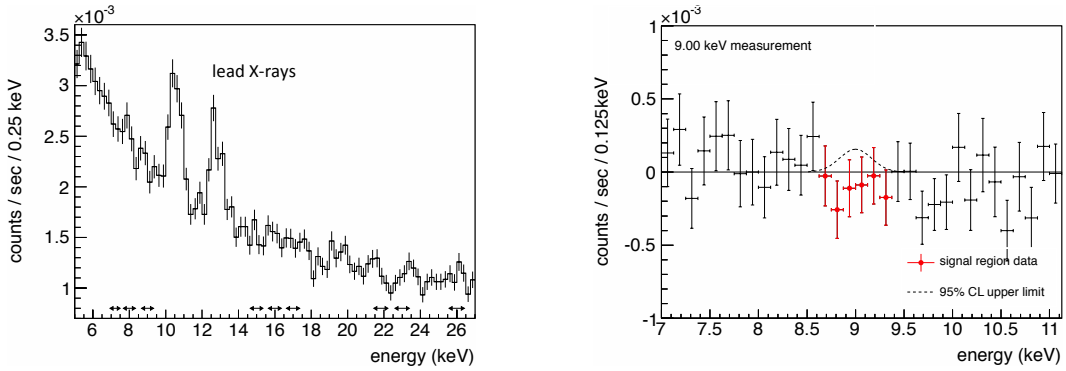

Figure 2: (left) Energy spectrum obtained with MBS closed (BG spectrum). Arrows show regions in which paraphoton searches are performed. (right) Energy spectrum measured at $\omega = 9.00$ keV. Background contributions are subtracted. Signals with statistical errors are shown in cross, and dotted line shows obtained upper limit (95% C.L.) of the signal.

BG spectrum (Fig. 2 (left)) is measured from 16th to 17th June with MBS closed. The other setup including the lead shields are completely the same as in the paraphoton searches. Total livetime of BG measurement is 1.6×10^5 s. The BG rate at 7.00 keV is $(10.9 \pm 0.3) \times 10^{-3}$ s^{-1} keV^{-1} and gradually decreases toward $(4.6 \pm 0.2) \times 10^{-3}$ s^{-1} keV^{-1} at 26.00 keV. No apparent structure is observed in the measured BG spectrum except for 10.6 keV and 12.6 keV, X–rays from the lead shields.

Signal region is defined as inside $\pm 2\sigma$ around the beam energy ω. Since signal regions are not overlapped among all measurements, the BG spectrum is commonly used for all subtractions (Fig. 2 (right)). The subtracted signal rates (ΔN) are also shown in Tab. 1, and no significant excess is observed for all 9 measurements. Using these rates, we set upper limits on signal rates of measurements. Gaussian distributions are assumed from center values and the standard deviations of ΔN, and 95% C.L. positions in the physical (i.e. positive) regions are set as a signal upper limit (ΔN_{95}). Finally, the upper limits on the LSW probability (P_{95}) are obtained by $\Delta N_{95}/\epsilon I$.

Vertical profile of the X–ray beam ($\rho(x)$) has to be taken into account in order to translate P_{95} to the limit on the mixing parameter χ, Since the incident angles of the beam into the second crystal of the monochromator and the first mirror are very shallow, $\rho(x)$ affects the lengths of the oscillation regions. As a result, these lengths are smeared by $\rho(x)$, and the LSW probability is written as,

$$P = \int_x \rho(x)\, p_{\gamma\to\gamma'}\left(L_1\left(x\right)\right)\, p_{\gamma'\to\gamma}\left(L_2\left(x\right)\right)\, \mathrm{d}x. \tag{2}$$

Here, $L_1(x)$ is the length of photon $\rightarrow$ paraphoton oscillation region modified by the vertical position, and $L_2(x)$ is that of the re-oscillation region. The integration is numerically calculated for each ω as a function of $m_{\gamma'}$, and P_{95} is translated to the limit on χ. Figure 3 shows 95% C.L. limit obtained using a data set of 9.00 keV measurement, and upper side of the line is excluded. The limit is smoothed by the smearing effect of $\rho(x)$ and becomes constant for masses from 5 eV up to around 9 keV (labeled as "(b)").

A combined result of 9 measurements rules out the limit oscillations in the region (a), and

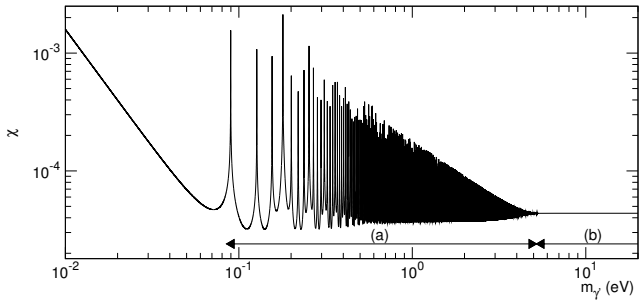

Figure 3: Upper limit (95% C.L.) on χ as a function of paraphoton mass ($m_{\gamma'}$) obtained with only one search at $\omega = 9.00$ keV. Spiky structure is due to the photon–paraphoton oscillation as shown in Formula (1). Spikes are smeared for heavier mass region (labeled as "(b)"), because of the smearing effect in Formula (2).

is shown in Fig. 4 with other results. Conservatively, the worst value around 1.39 eV represents our result (see [11] for details),

$$\chi < 8.06 \times 10^{-5} \quad (95\% \text{ C.L.}). \tag{3}$$

This result is valid for masses up to 26 keV, the maximum beam energy of our search. Our result is the most stringent for masses around eV region as a terrestrial search.

4 Summary and prospects for the next phase

We performed a paraphoton search for the first time with intense X–ray beams at SPring–8 synchrotron radiation facility. A double oscillation process, "photons oscillating into paraphotons and oscillating back into photons", is assumed, and photons passing through a wall are searched. No such photons are observed, and a new limit on the photon–paraphoton mixing angle, $\chi < 8.06 \times 10^{-5}$ (95% C.L.) is obtained for 0.04 eV $< m_{\gamma'} <$ 26 keV. The result provides the most stringent laboratory constrains on paraphotons, and extends the mass region probed with LSW methods up to X–ray region.

Based on this backgrounds obtained from the first phase, a detailed planning for the next-phase paraphoton search has already started. An intense X–ray beam from a *free electron laser* (FEL) is used instead as a pulsed X–ray source. SACLA[12] is one of such FEL facility located next to SPring-8, and started its public use since last year. It provides pulsed beams with 60 Hz and a pulse width of less than 10 fs.

A time window of the detector, which coincides with the pulsed beam is expected to reduce currently observed environmental BGs to zero. Resulting improvement of S/N is about 2 orders of magnitude compared to the first result for one week measurement. An expected limit for the phase 2 is also shown in Fig. 4.

Acknowledgements

The synchrotron radiation experiment is performed at BL19LXU in SPring–8 with the approval of RIKEN (Proposal No. 20120088). Sincere gratitude is also expressed to Dr. Suehara and

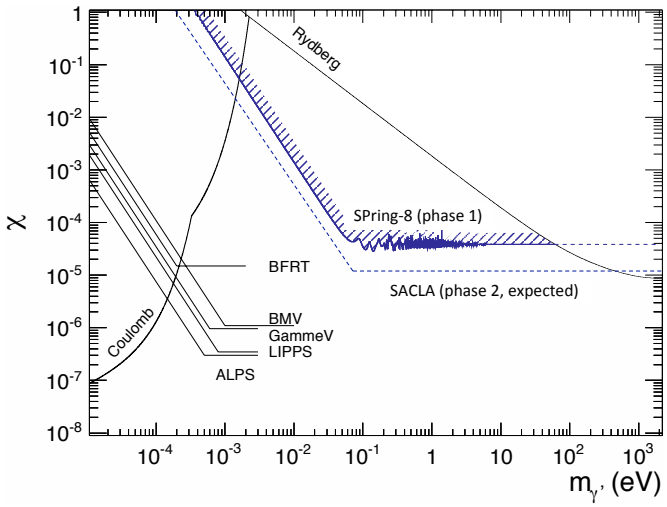

Figure 4: 95% C.L. limit on the paraphoton mixing angle obtained from our first result (SPring-8) compared with other laboratory experiments. Rydberg is a limit from the measurement of Rydberg atoms [9], Coulomb is from the Coulomb low confirmation [10], and BFRT, BMV, GammeV, LIPPS, and ALPS are from LSW experiments using optical laser [6]. An expected limit of our next phase is also shown as SACLA phase 2.

Mr. Ishida for useful discussions. Work of T. Inada is supported in part by Advanced Leading Graduate Course for Photon Science (ALPS) at U. Tokyo.

References

[1] J. Jaeckel and A. Ringwald, Ann. Rev. Nucl. Part. Sci. 60 (2010) 405.

[2] B. Holdom, Phys. Lett. B 166 (1986) 196.

[3] L. B. Okun, JETP 56 (1982) 502.

[4] K. Van Bibber *et al.*, Phys. Rev. Lett. 59 (1987) 759.

[5] S. L. Adler *et al.*, Ann. Phys. 323 (2008) 2851.

[6] BFRT Collaboration, R. Cameron *et al.*, Phys. Rev. D 47 (1993) 3707;
BMV Collaboration, M. Fouche *et al.*, Phys. Rev. D 78 (2008) 032013;
GammeV Collaboration, A. Chou *et al.*, Phys. Rev. Lett. 100 (2008) 080402;
LIPPS Collaboration, A. Afanasev *et al.*, Phys. Lett. B 679 (2009) 317;
ALPS Collaboration, K. Ehret *et al.*, Phys. Lett. B 689 (2010) 149.

[7] ADMX Collaboration, A. Wagner *et al.*, Phys. Rev. Lett. 105 (2010) 171801;
M. Betz and F. Caspers, Conf. Proc. C 1205201 (2012) 3320.

[8] M. Yabashi *et al.*, Nucl. Instrum. Meth. A 467-468 (2001) 678.

[9] R. G. Beausoleil *et al.*, Phys. Rev. A 35 (1987) 4878.

[10] E. R. Williams, J. E. Faller and H. A. Hill. Phys. Rev. Lett. 26 (1971) 721.

[11] T. Inada *et al.*, Phys. Lett. B 722 (2013) 301.

[12] T. Ishikawa *et al.*, Nat. Photonics. 6 (2012) 540.